Published in final edited form as:
Biochemistry. 2009 July 7; 48(26): 6249–6258. doi:10.1021/bi900373x.

Transmembrane Helix 12 Modulates Progression of the ATP Catalytic Cycle in ABCB1†

Emily Crowley[‡], **Megan L. O'Mara**[§,‖], **Catherine Reynolds**[‡], **D. Peter Tieleman**[§], **Janet Storm**[‡], **Ian D. Kerr**[⊥], and **Richard Callaghan**[*,‡]

[‡]Nuffield Department of Clinical Laboratory Sciences, John Radcliffe Hospital, University of Oxford, Oxford OX3 9DU, United Kingdom

[§]Department of Biological Sciences, University of Calgary, 2500 University Drive, Northwest Calgary, Alberta T2N 1N4, Canada

[‖]Molecular Dynamics Group, School of Chemistry and Molecular Biosciences, University of Queensland, Brisbane, Queensland 4072, Australia

[⊥]Centre for Biochemistry and Cell Biology, School of Biomedical Sciences, University of Nottingham, Queen's Medical Centre, Nottingham NG7 2UH, United Kingdom

Abstract

Multidrug efflux pumps, such as P-glycoprotein (ABCB1), present major barriers to the success of chemotherapy in a number of clinical settings. Molecular details of the multidrug efflux process by ABCB1 remain elusive, in particular, the interdomain communication associated with bioenergetic coupling. The present investigation has focused on the role of transmembrane helix 12 (TM12) in the multidrug efflux process of ABCB1. Cysteine residues were introduced at various positions within TM12, and their effect on ATPase activity, nucleotide binding, and drug interaction were assessed. Mutation of several residues within TM12 perturbed the maximal ATPase activity of ABCB1, and the underlying cause was a reduction in basal (i.e., drug-free) hydrolysis of the nucleotide. Two of the mutations (L976C and F978C) were found to reduce the binding of [γ-^{32}P]-azido-ATP to ABCB1. In contrast, the A980C mutation within TM12 enhanced the rate of ATP hydrolysis; once again, this was due to modified basal activity. Several residues also caused reductions in the potency of stimulation of ATP hydrolysis by nicardipine and vinblastine, although the effects were independent of changes in drug binding per se. Overall, the results indicate that TM12 plays a key role in the progression of the ATP hydrolytic cycle in ABCB1, even in the absence of the transported substrate.

ABCB1 (P-glycoprotein) is a member of the ATP binding cassette (ABC) protein family and functions as a multidrug efflux pump. Expression of ABCB1 is found in numerous types of drug-resistant cancers and also a number of endogenous tissues. The physiological role of ABCB1 involves regulating the excretion of xenobiotics from the liver and the gastrointestinal tract and a protective role at the blood–brain barrier and testes (1-3). The protein is referred to as a multidrug transporter because it recognizes and transports an astonishing array of chemically and functionally distinct compounds. Malignant cells exploit

†This investigation was generously supported by a Cancer Research U.K. Studentship to E.C. (C362/A5502), for which R.C. was the principal investigator. M.L.O. was supported by a fellowship from the Canadian Institutes of Health Research (CIHR). D.P.T. is an AHFMR Senior Scholar and CIHR New Investigator. Work in D.P.T.'s group is supported by CIHR.

*To whom correspondence should be addressed. Telephone: +44-(0) 1865-221-110. Fax: +44-(0)1865-221-834. richard.callaghan@ndcls.ox.ac.uk..

Europe PMC Funders Author Manuscripts

multidrug transporters, such as ABCB1, to evade the cytotoxic effects of chemotherapy, a phenomenon known as multidrug resistance (MDR) (4, 5). Inhibiting multidrug transporters could restore the efficacy of chemotherapy in drug-resistant cancers (6).

Unfortunately, little is known about the location and structural features of drug binding sites despite over 30 years of research, thereby making rational drug design of inhibitors problematic (6). The inherent promiscuity of ABCB1 makes it difficult to determine the location of the drug binding sites (6, 7), although at least four sites have been identified within the transmembrane (TM) helices of the transporter (8-11). Recent investigations by Loo and colleagues suggest that TM1 and TM7 contribute to the drug binding pocket of ABCB1, although these results specifically pertain to the modulator verapamil (12, 13). In contrast, the interfacial regions between TM5/TM8 and TM3/TM11 appear to be important for the interaction of propafenone-type ABCB1 inhibitors (14). Further biochemical and structural studies are required to fully ascertain the location of drug binding sites on ABCB1.

Because drug translocation at the transmembrane domains (TMDs) and ATP hydrolysis at the nucleotide binding domains (NBDs) must be coordinated for active efflux, interdomain communication is critical and appears to work in both TMD → NBD and NBD → TMD directions by virtue of conformational changes within the protein. Global conformational changes in the TMDs have been observed upon nucleotide binding, as shown by cryo-electron microscopy, differential protease digestion, and the altered accessibility of cysteine residues (in the TMDs) and antibodies recognizing extracellular epitopes on the protein (15-21). The importance of such NBD → TMD communication has also been emphasized by the fact that the impetus for drug release (i.e., altering the binding site from an inward, high-affinity to an outward, low-affinity conformation) is derived from nucleotide binding (22, 23). In the TMD → NBD direction, the “sluggish” basal rate of ATP hydrolysis has been shown to increase in the presence of drugs as a consequence of an “accelerated” engagement of the NBDs to create the nucleotide sandwich dimer (15-18, 24). In this state, ATP is locked between the ABC signature motif of one NBD and the Walker A and B motifs of the other NBD (25-28). Furthermore, scanning mutagenesis revealed that a number of residues in the TMDs significantly affected the rate of ATP hydrolysis in the NBDs (29-31). Clearly, communication between the TMDs and the NBDs is critical for the coupling of nucleotide hydrolysis and drug efflux.

Our understanding of the communication pathway(s) that coordinate drug binding and ATP hydrolysis to allow for drug transport and the location of sites to which drugs bind in ABCB1 is limited, and many fundamental questions remain unanswered. Early attempts to isolate the drug binding sites suggested that TM6 and TM12 were integrally involved in the translocation mechanism of ABCB1. Additional approaches to elucidate the role of these helices involved (i) genetic manipulation, (ii) mass spectrometry, (iii) cysteine-scanning mutagenesis, (iv) attachment of photolabile substrates, (v) introducing intraprotein cross-links, and (vi) cytotoxicity studies (5, 21, 29, 31-36). These investigations highlighted the significance of TM helices 6 and 12 in contributing in some manner to the transport process by mediating interdomain communication, the translocation pathway, or possibly drug binding per se. Topographical analysis of TM6 at various stages of the catalytic cycle has revealed a number of residues undergoing conformational transitions. The data suggested the presence of a central pivot about which conformational changes are transmitted to the NBDs (37, 38). Homology modeling approaches concurred with this data, which is commensurate with the direct physical link between TM6 and NBD1.

Clearly, our understanding of the role of TM helices 6 and 12 in the translocation mechanism of ABCB1 is progressing. The present investigation focuses on the functional

involvement of residues in TM12 through perturbation of the helix by cysteine-directed mutagenesis. The effects of mutations were examined on basal and drug-stimulated ATP hydrolysis, as well as drug and nucleotide binding to ABCB1. Homology modeling was used to interpret the data and generate a further detailed understanding of this key helix in the multidrug translocation mechanism.

MATERIALS AND METHODS

Materials

Octyl-β-D-glucoside, C219 antibody, and Ni-NTA His Bind Superflow resin were obtained from Merck Chemicals Ltd. (Nottingham, U.K.). Dimethylsulfoxide (DMSO), disodium adenosine triphosphate (Na_2ATP), cholesterol, vinblastine, and nicardipine were all from Sigma (Poole, U.K.). Crude *Escherichia coli* lipid extract was obtained from Avanti Polar Lipids (Alabaster, AL). Insect-Xpress medium was purchased from Lonza Ltd. (Wokingham, U.K.), and Excell 405 was purchased from SAFC Biosciences (Andover, U.K.). [γ-^{32}P]-Azido-ATP (430–740 GBq/mmol) was purchased from Affinity Labeling Technologies (Lexington, KY), and [^{125}I]-iodo-aryl-azido-prazosin (81.4 TBq/mmol) was obtained from Perkin-Elmer LAS (Boston, MA).

Site-Directed Mutagenesis of TM12 in ABCB1: Introduction of Cysteines

Mutants were constructed using Quik-Change (Stratagene) or Altered Sites II (Promega) mutagenesis systems with a pAlter- or pFastBac1-MCHS template. The MCHS cDNA encodes an ABCB1 isoform devoid of cysteines with a C-terminal hexa-histidine tag, which has been described previously (15, 39). Mutagenic oligonucleotides were designed to contain the cysteine codon TGC or TGT and a silent restriction enzyme site (Table 1). Mutants were identified by diagnostic restriction digest, and if the mutant was generated in pAlter, a cDNA fragment containing the desired mutation was subcloned into pFastBac1-MCHS to produce the required construct. The mutant plasmids were sequenced (Biochemistry, University of Oxford) to ensure the fidelity of mutagenesis.

Expression, Purification, and Reconstitution of ABCB1

Recombinant baculovirus was generated using the Bac-to-Bac baculovirus expression system according to the instructions of the manufacturer (Invitrogen). *Trichoplusia ni* (high-five) cells were infected with recombinant baculovirus at a multiplicity of infection of 5 expressing mutant isoforms of ABCB1 were harvested 3 days post-infection by centrifugation (2000*g* for 10 min). For comparative analysis of protein expression, 2×10^6 cells were resuspended in phosphate-buffered saline supplemented with 2% (w/v) sodium dodecyl sulfate (SDS) and proteins were resolved by SDS–polyacrylamide gel electrophoresis (PAGE). ABCB1 was detected with the C219 antibody following immunoblotting (40). For large-scale expression of ABCB1 isoforms, 1.5×10^9 cells were infected and cell membranes were isolated 72 h post-infection as previously described and stored at −80 °C for up to 1 year (15, 39). Purification by immobilized metal-affinity chromatography and reconstitution was achieved using techniques previously described (15, 39). Confirmation of reconstitution involved the analysis of lipid and protein co-migration through sucrose density gradients. The protein concentration following reconstitution was determined using an adapted Lowry colorimetric assay with bovine serum albumin as a standard (DC-Brad Protein Assay, BioRad) (41). This necessitated the centrifugation (100000*g* for 30 min) of 500 μL of purified, reconstituted ABCB1 and resuspension of the pellet in 50 μL of water to remove buffer contaminants (specifically imidazole) that interfere with protein analysis.

Partial Proteolysis of ABCB1 by Trypsin

Partial proteolysis of each mutant isoform was performed to verify that the single cysteine mutants were expressed in the correct conformational state in the membrane. To remove protease inhibitors from the sample, 150 μL (approximately 5 μg) of purified, reconstituted protein was centrifuged at 100000*g* for 30 min and the pellet was resuspended in buffer (50 mM Tris-HCl at pH 7.4, 150 mM NH_4Cl, 5 mM $MgSO_4$, and 0.02% NaN_3). The sample was incubated at 37 °C with 0.5 μg of bovine pancreatic trypsin in 20 mM Tris-HCl at pH 7.7. The reaction was stopped after 0, 2, 4, 6, 8, 10, and 15 min by the addition of 7.2% (w/v) trichloroacetic acid and 0.015% (w/v) sodium deoxycholate. The precipitated protein was resuspended in 20 μL of a 1:1 solution of 4× Laemmli sample buffer and TCA resuspension buffer [100 mM Tris base, 3 mM dithiothreitol (DTT), and 3% SDS at pH 11] and resolved by 10% (v/v) SDS–PAGE. ABCB1 and the digested fragments were detected using the C219 antibody following immunoblotting. The positive control corresponds to protein in the absence of proteolytic digestion.

ATPase Activity of Purified, Reconstituted ABCB1 Isoforms

The ATP hydrolytic activity of purified, reconstituted ABCB1 was determined by measuring the release of inorganic phosphate using a modified colorimetric assay developed by Chifflet et al. (15, 39, 42). Michaelis–Menten parameters were determined by incubating proteoliposomes (0.9–1.5 μg) with varying concentrations of Mg·ATP (0–2 mM) in the presence or absence of nicardipine or vinblastine (30 μM), as previously described (15). To determine the potency of drugs to stimulate ATP hydrolysis, proteoliposomes were incubated with a constant Mg·ATP concentration (2 mM) and varying nicardipine and vinblastine concentrations (15).

[γ-^{32}P]-8-Azido-ATP Binding to Purified, Reconstituted ABCB1 Isoforms

Nucleotide binding to P-glycoprotein was assessed by photoactive labeling of purified, reconstituted protein with [γ-^{32}P]-8-azido-ATP (38). Proteoliposomes (0.3 μg) were incubated with [γ-^{32}P]-8-azido-ATP (concentrations up to 100 μM) in a total volume of 30 μL on ice for 10 min under subdued lighting and then subjected to UV irradiation (100 W, 5 cm, λ = 265 nm) for 8 min. Post-irradiation, the protein was precipitated using 7.2% (w/v) trichloroacetic acid and 0.015% (w/v) sodium deoxycholate. The precipitated protein was resuspended in 20 μL of a 1:1 solution of 4× Laemmli sample buffer and TCA resuspension buffer (100 mM Tris base, 3 mM DTT, and 3% SDS at pH 11) and resolved by 7.5% (v/v) SDS–PAGE. Labeling was detected by autoradiography at −80 °C using Biomax Film (Kodak). The interaction of ATP and ADP with the protein was determined in the presence of 10 μM [γ-^{32}P]-azido-ATP and 1 mM unlabeled nucleotide.

Statistical Analysis

All data analyses were performed using GraphPad Prism, version 4. A comparison of data sets for each isoform was performed using analysis of variance (ANOVA), applying Dunnett's test, where significance was determined by a p value<0.05.

Homology Modeling

The pre-equilibrated ATP-bound closed-state ABCB1 homology model developed by O'Mara and Tieleman (44), embedded in a palmitoyloleonyl-phosphatidyl-ethanolamine (POPE) lipid bilayer was used as the initial ABCB1 conformation in this analysis. A series of single *in silico* cysteine point mutations were introduced into TM12 using DeepView (45) at residues L976, F978, A980, V988, G989, and Q990 to give a series of six lipid-embedded single-point mutation ABCB1 models. The models were energy-minimized as previously described (44).

RESULTS

In the current study, we wished to address the role of TM12 in the ATP catalytic cycle of ABCB1. To do this, we constructed a series of single cysteine isoforms of ABCB1. Residues were identified for mutation based on a direct comparison of the sequences of TM6 and TM12 and by inspection of our Sav1866-directed homology model of human ABCB1 (44). The 11 single cysteine isoforms generated provide both a longitudinal and rotational coverage of the α helix.

Expression of ABCB1 Mutant Isoforms in High-Five Cells

ABCB1 single cysteine mutants were expressed in highfive cells to carry out detailed biochemical investigations on purified protein. Figure 1 is a representative immunoblot showing expression of each of the 11 single cysteine mutants in insect cells following baculoviral infection. The amount of protein expressed varied with different batches and ages of recombinant baculovirus, but none of the isoforms displayed consistently reduced or elevated expression levels. In any case, all analyses used purified ABCB1, and activities were normalized to equivalent amounts of protein.

Purification of ABCB1 Isoforms and Characteristics of ATP Hydrolysis

The extraction and purification of ABCB1 from insect cell membranes has previously been described (39), and in the present study, the protein purity was 80–90%, with approximately 90% of the protein being eluted at 120 mM imidazole, as shown in Figure 2. Successful reconstitution for each mutant isoform was routinely assessed by tracking the comigration of protein and radiolabeled lipids ([^{3}H]-PC) through a sucrose density gradient. Reconstitution efficiency did not vary between the ABCB1 mutants, and preparations where<80% of the protein did not co-migrate with lipids were discarded from subsequent analyses.

A prerequisite for the successful purification of each mutant isoform is the correct trafficking of the protein to the cell membrane following expression in insect cells. However, to verify that each single cysteine mutant adopted the correct conformational state in the membrane, partial proteolysis of the mutant isoforms was carried out using the protease trypsin. Panels B and C of Figure 2 show a time course of proteolytic digestion of the purified, reconstituted Cys-less and M986C proteins. No discernible difference in the fragment sizes was detected following the proteolysis of each ABCB1 mutant isoform when compared to the Cys-less control (data not shown).

Cysteine-less ABCB1 displayed Michaelis–Menten characteristics in ATP hydrolysis as shown in Figure 3A. The ATPase activity was measurable even in the absence of transported substrate (i.e., basal activity) with a V_{max} = 111 ± 23 nmol min^{-1} mg^{-1} and an affinity constant (K_M) for ATP=0.37 ± 0.06 mM. In the presence of the modulator nicardipine (30 μM), the ABCB1 activity was stimulated to a V_{max}=561 ± 68 nmol min^{-1} mg^{-1} (K_M=0.38 ± 0.03 mM). The transported substrate vinblastine (30 μM) also stimulated ATP hydrolysis; however, the degree of stimulation was only approximately 2-fold, thereby generating a V_{max}=248 ± 37 nmol min^{-1} mg^{-1} (K_M=0.40 ± 0.05 mM). Full dose–response analyses of the two drugs were also undertaken to generate estimates of the potency and degree of stimulation, as shown in Figure 3B. Nicardipine produced 4.0 ± 0.6-fold stimulation with a potency of EC_{50} = 4.0 ± 0.6 μM, while the degree of stimulation by vinblastine was 2.2 ± 0.2-fold with an EC_{50}=5.9 ± 2.9 μM.

Effects of Mutations in TM12 on ATPase Activity of ABCB1

The Michaelis–Menten characteristics of each mutant isoform of ABCB1 were determined, and the maximal activities were plotted under basal conditions (Figure 4A) or in the

presence of nicardipine (Figure 4B) or vinblastine (Figure 4C). The most striking alterations were the approximately 5-fold reductions in basal ATPase activity for the L976C (V_{max}=26 ± 4 nmol min^{-1} mg^{-1}) and F978C (V_{max}=27 ± 9 nmol min^{-1} mg^{-1}) mutations compared to the control cysteine-less isoform of ABCB1. There were also less dramatic (40%) reductions in the basal activities of the V988C (V_{max} = 66 ± 4 nmol min^{-1} mg^{-1}) and Q990C (V_{max}=61 ± 12 nmol min^{-1} mg^{-1}) mutations. These latter two residues correspond to the region 346–348 in TM6, an area that was also sensitive to mutation (38). In complete contrast, the A980C mutation in TM12 caused an increase in the basal ATPase activity (V_{max}=203 ± 40 nmol min^{-1} mg^{-1}) compared to the cysteine-less isoform. None of the mutations in TM12 affected the affinity constant for ATP, and the perturbations in basal hydrolysis imply a fundamental involvement for TM12 in the progression of the catalytic cycle of ABCB1.

A number of mutant isoforms of ABCB1 also displayed perturbations in the V_{max} values for ATP hydrolysis in the presence of nicardipine. Inspection of Figure 4B indicates that residues with altered activity in the presence of nicardipine were similar to those with modified basal ATP hydrolysis. L976C (V_{max}=231 ± 80 nmol min^{-1} mg^{-1}), F978C (V_{max}=142 ± 40 nmol min^{-1} mg^{-1}), V988C, G989C, and Q990C all caused statistically significant (p<0.05) reductions in the V_{max} values for nicardipine-stimulated ATPase activities (Figure 4B). Again, in contrast, the nicardipine-stimulated activity of the A980C isoform was almost 3-fold higher (V_{max}=1352 ± 50 nmol min^{-1} mg^{-1}) than observed for the cysteine-less control.

Such altered ATPase activities in the presence of nicardipine could reflect modified drug–protein interactions, which we examined with full dose–response curves (Table 2). For the majority of residues showing altered ATPase V_{max} values, the interaction with nicardipine was unaltered as determined by the potency (EC_{50}) and the fold stimulation of ATPase activity. Consequently, the altered V_{max} values in the presence of nicardipine are likely to be the result of the perturbation of the basal activity caused by the mutations. However, the F978C isoform did display an altered nicardipine–ABCB1 interaction; that is, the potency of nicardipine was reduced from 4.1 ± 1.1 to 24.1 ± 2.3 μM.

Vinblastine also stimulates the ATPase activity of ABCB1. Moreover, this drug binds at a site distinct from that of nicardipine, and furthermore, the mutation of residues in TM6 produced distinct effects on the stimulation of ATPase activity by nicardipine and vinblastine, suggesting different routes of TMD–NBD communication by the two drugs. However, Figure 4C and Table 2 indicate that mutations in TM12 produced similar effects on vinblastine stimulation to those with nicardipine. For example, mutations L976C, F978C, V988C, and Q990C all displayed statistically significant reductions in maximal ATPase activity in the presence of vinblastine compared to the control cysteine-less isoform. However, of these, only the F978C isoform again displayed a reduction in the potency for stimulation of its ATPase activity by vinblastine, although the degree of stimulation remained unaffected.

There was, however, a drug-dependent difference on the stimulation of ATPase activity observed with the G984C and M986C isoforms (Table 2). For G984C, nicardipine was associated with a reduction in potency and degree of stimulation, whereas the influence of vinblastine was similar to that in cysteine-less ABCB1. In contrast, for the M986C isoform, the effects of nicardipine were similar to cysteine-less ABCB1, while the potency of vinblastine was significantly (p<0.05) reduced. Consequently, there were some drug-specific effects of the mutations in TM12, although the frequency was less than previously observed in TM6 (15, 38).

In summary, the data reveal that ATPase activity is affected by mutations within TM12. Excluding the A980C isoform, which displayed enhanced ATPase activity, the effects were primarily a reduction of ATP hydrolysis. Although the ATPase activity in the presence of nicardipine and vinblastine was modified, the potency and degree of stimulation were, with a few exceptions, largely unaffected. The underlying effect of the mutations in TM12 appears to be a modification of the basal ATP hydrolytic process by ABCB1.

Nucleotide Binding Characteristics of Functionally Perturbed Mutants

What is the underlying cause of the perturbation in the basal ATPase activity in the TM12 mutant isoforms? ATPase activity is a multistep process involving (i) binding of ATP, (ii) hydrolysis of nucleotide, and (iii) release of ADP and inorganic phosphate. To determine whether ATP binding is affected in mutants with reduced ATPase activity, the extent of labeling by the photoactivatable ATP analogue [γ-^{32}P]-azido-ATP was examined. Assay conditions (i.e., T=4 °C) precluded nucleotide hydrolysis by the proteins and therefore enabled measurement of the binding event. Figure 5A presents a representative autoradiogram of [γ-^{32}P]-azido-ATP binding to the mutants L976C, F978C, A980C, V988C, G989C, and Q990C. Quantitative analysis of the extent of binding in the presence and absence of ATP and ADP was analyzed by densitometry, and the data are summarized in Table 3. The results indicate that at a concentration of 10 μM [γ-^{32}P]-azido-ATP there was a discernible difference between the binding of the ATP analogue to L976C, F978C, and A980C. Mutant isoforms L976C and F978C displayed a 4- and 15-fold decrease in binding, whereas A980C showed a 1.8-fold increase in binding at the concentration of [γ-^{32}P]-azido-ATP used. In contrast, the V988C, G989C, and Q990C isoforms did not show a statistically significant reduction in the degree of [γ-^{32}P]-azido-ATP photolabeling, despite their reduced ATPase activity (see above).

To further investigate the differences, binding was measured at a range of [γ-^{32}P]-azido-ATP concentrations. Figure 5B shows the autoradiography data obtained for [γ-^{32}P]-azido-ATP photolabeling of the cysteine-less and L976C isoforms of ABCB1. Figure 5C shows the densitometric analysis of the dose–response curve for the cysteine-less, A980C, L976C, and F978C isoforms. At the range of [γ-^{32}P]-azido-ATP concentrations studied, there was no discernible difference between the labeling of cysteine-less (B_{max}=1.00, K_D=25 μM) and A980C (B_{max}=1.21, K_D=23 μM) isoforms of ABCB1. In contrast, the mutant isoforms L976C (B_{max}=0.24, K_D=17 μM) and F978C (B_{max}=0.19, K_D=17 μM) displayed 4–5-fold reductions in the amount of [γ-^{32}P]-azido-ATP binding compared to the cysteine-less control.

Therefore, the decrease in basal and drug-stimulated ATPase activity observed for the L976C and F978C isoforms can be explained at least in part by impaired ATP binding at the NBDs. However, mutant A980C, which was characterized by a significantly higher ATPase activity, did not show any appreciable changes in nucleotide binding.

In Silico Characterization of TM12 Functionally Perturbed Mutants

Despite 45% sequence identity between TM6 and TM12, there appears to be little functional symmetry. That is, the functional effects of mutations in TM12 do not mirror the effects previously characterized in TM6 mutants (15, 38). To investigate whether such differences are a reflection of a physical asymmetry between the helices and their surroundings, we attempted to rationalize three of the functionally perturbed TM12 single cysteine mutants (i.e., F978C, A980C, and V988C) by reference to a molecular model of ABCB1. We have previously used molecular modeling to explore the effects of mutations on ABCB1 function and have continued that approach here, using our published model of human ABCB1 in the ATP-bound state. The recently published medium-resolution structure of mouse ABCB1 in

the open apo conformation (46) has enabled us to confirm the position and orientation of the native TM6 and TM12 residues. While the conformational differences between the crystal structure and the ATP-bound model prevent a direct comparison of residues involved in interhelical interactions, we found the position on the helix and orientation of the residues modeled corresponded to the crystal structure, supporting the ATP-bound ABCB1 homology model. The six TM12 mutations that result in a functional perturbation of ATPase activity produce either an increase or a decrease in ATPase activity. Of the six mutations, only A980C resulted in increased ATPase activity. Visualization of the ABCB1 homology model shows that the side chain of the native A980 (Figure 6A) has no interactions with residues outside of TM12. *In silico* mutation to 980C lengthens the side chain, allowing hydrogen bonding with the backbone of S850 and resulting in an increase in the number of interhelix contacts between TM12 and TM9 (Figure 6B). Because both TM9 and TM12 make direct contact with NBD2, we infer that the increase in contacts between the two helices allows for a more concerted communication to NBD2 and accelerated ATPase activity.

The F978C mutation, located near the extracellular protein–lipid interface in the membrane-embedded region of TM12, is part of a conserved sequence motif present in TM12 and TM6. This mutation resulted in a significant decrease in the ATPase activity, nucleotide binding, and drug–protein interaction. The native F978 residue is located in a densely packed region of the protein, on a helix–helix interface, and interacts hydrophobically with F72 (TM1) (Figure 6C), contributing to TM12–TM1 helix–helix stabilization. The corresponding TM6 residue, F335, is involved in hydrophobic interactions with F732 from TM7, implying symmetry between TM6 and TM12. However, unlike the TM12 F978C mutation, the TM6 F335C mutation does not cause a significant reduction in ATPase activity (15). In TM12, mutation to the smaller 978C increases the distance between F978C and F72, preventing hydrophobic interactions (Figure 6D) and decreasing the number of TM12–TM1 contact points. The loss of the helix–helix interaction, in this instance, therefore contributes to a reduction in activity of ABCB1. Interestingly, the modeled mutation also alters the orientation of the F978C side chain, resulting in the complete exposure of the cysteine side chain into a pore below L975, which has been implicated in dibromobimane binding (47).

Cysteine mutagenesis of V988 resulted in decreased ATPase activity, without marked perturbations in drug and nucleotide affinity. In the model, V988 is located on the lipid-accessible surface of the protein in a cleft between TM9 and TM10, where it forms a trimeric β-branched stabilization point with I868 (TM10) and M949 (TM11). Mutation to V988C disrupts the hydrophobic interaction with I868 from TM9, and the V988C side chain is oriented toward the TM10 residue M949. This region is highly conserved in TM6, but despite V345, the analogous residue to V988, making similar β-branched hydrophobic interactions with respective helices, when mutated to cysteine, it caused no functional perturbation (37, 38) (Figure 7A). This further highlights the functional asymmetry between TM6 and TM12.

DISCUSSION

Over 15 years ago, mutations within TM12 and TM6 demonstrated that these helices alter the drug-resistance profile of ABCB1 and therefore presumably play a role in the translocation process. This investigation highlights the importance of TM12 in coordinating drug-binding events with the process of nucleotide hydrolysis in ABCB1 and furthers our understanding of the mechanism of coupling in this transporter.

In the present investigation, we made a series of mutations to ABCB1, which positioned a unique cysteine residue along the length of TM12 and provided coverage of the helical surface. We demonstrated that a number of these mutations had a dramatic effect on the basal activity of ABCB1. A similar study with TM6 revealed significantly fewer positions at which site-directed mutagenesis to cysteine caused functional perturbation in the basal state (notably mutant isoform G346C). The most dramatic effects in TM12 were observed in residues at the extracellular (L976C and F978C) and intracellular (V988C and Q990C) ends of the helix. The V988C and Q990C mutations reduced basal ATPase activity without any significant change in nucleotide binding per se. This implies that the altered helical properties caused by site-directed mutagenesis modulated the conformational communication route between the transmembrane and nucleotide binding domains.

In contrast, the reduced basal activity observed with mutants L976C and F978C appeared to be a consequence of reduced nucleotide binding. This is unexpected because both residues lie at the extracellular end of the helix at a considerable distance from the site of nucleotide binding and hydrolysis. This finding illustrates the cooperativity between these two domains and the coupling required to generate drug translocation, as previously demonstrated using a range of experimental approaches (17, 23, 24, 48-52). In particular, it highlights the importance of TM12 in coordinating conformational transitions within the NBDs to enable association of ATP.

Consistent with previous findings, there are a number of drugspecific effects caused by the mutation of certain residues in TM12 to cysteine. Mutant G989C did not affect vinblastine-stimulated activity but markedly reduced the degree and potency of stimulation by nicardipine. Both nicardipine and vinblastine have previously been shown to interact at pharmacologically distinct sites (9, 53), suggesting that mutant G989C is involved in communicating nicardipine but not vinblastine binding to the NBDs. In contrast, mutation of the equivalent residue (G346C) in TM6 was implicated in communication between the vinblastine binding site and the NBDs (37). The data continue to support our assertion that drugs communicate to the NBDs via distinct pathways and that allosteric communication between TMD1 and TMD2 to NBD1 and NBD2 is not symmetrical in ABCB1.

TM12 is clearly sensitive to cysteine mutagenesis in a way quite dissimilar to TM6. The ABCB1 homology model was therefore used to explore the basis for functional perturbations caused by site-directed mutagenesis in TM12. We hypothesize from analysis of the model that the packing of TM12 to neighboring helices is optimized to propagate structural changes to the remainder of the protein. Mutations of residues that disturb the interhelical packing will result in alterations to the ATPase activity. However, there is an additional dissimilarity between TM6 and TM12 evident from the model, which could contribute to the functional asymmetry discussed here. Previous analysis suggested that TM6 contains a hinge region in the central part of the membrane introduced by the presence of three adjacent β-branched amino acids, which disrupt the helical hydrogen-bonding pattern (Figure 7A). In contrast, the modeled TM12 helix in the ABCB1 homology model shows no disruption of the α-helical hydrogenbonding pattern in the analogous region, with an unbroken, typical α-helical hydrogen-bonding pattern along the helix length from the extracellular water–lipid interface to the membrane-embedded cytoplasmic region of TM12 (Figure 7B). Instead, the modeled TM12 showed a marked kink near the intracellular lipid–water interface. The sequence motif SSFAPD (S992–D997) provides the demarcations of the modeled kink. The recently published crystal structure of mouse ABCB1 also contains a marked kink in TM12, located toward the intracellular aspect of TM12 (46) (Figure 8). Of particular note is the conserved sequence motif SSFAPD (V988–S993 in the mouse sequence), which delineates the helical disruption in the crystal structure, adding confidence to the homology model. Neither the crystal structure or homology model show a marked

kink in TM6. Perhaps this relative “rigidity” of the TM12 helix (compared to TM6) renders it more sensitive to perturbations by site-directed mutagenesis. This is reflected by the fact that the number of functional perturbations caused by site-directed mutagenesis in TM12 is greater than those in TM6. While the differing conformations of the apo ABCB1 crystal structure and ATP-bound homology model make a direct comparison of the two difficult, the absence of a marked TM6 kink in the recent ABCB1 crystal structure (46) and the correlation between the modeled and crystallographic asymmetries of TM6 and TM12 further support our postulated mechanism of action.

Clearly, the way in which TM6 and TM12 communicate to NBD1 and NBD2, respectively, is not symmetrical. Furthermore, functional asymmetry of the two NBDs (48) is not likely to be due to inherent properties of the NBDs themselves but due to differences in interdomain interactions. Despite there being distinct differences in the way that TM6 and TM12 communicate to the NBDs, as reflected by the differences in functional perturbations, perhaps the outcome is the same, i.e., to control hydrolysis and coordinate it such that drugs are translocated effectively.

REFERENCES

(1). Cordon-Cardo C, O’Brien JP, Casals D, Rittman-Grauer L, Biedler JL, Melamed MR, Bertino JR. Multidrug-resistance gene (P-glycoprotein) is expressed by endothelial cells at blood–brain barrier sites. Proc. Natl. Acad. Sci. U.S.A. 1989; 86:695–698. [PubMed: 2563168]

(2). Pavelic ZP, Reising J, Pavelic L, Kelley DJ, Stambrook PJ, Gluckman JL. Detection of P-glycoprotein with four monoclonal antibodies in normal and tumor tissues. Arch. Otolaryngol., Head Neck Surg. 1993; 119:753–757. [PubMed: 8100425]

(3). Smit JJ, Schinkel AH, Mol CA, Majoor D, Mooi WJ, Jongsma AP, Lincke CR, Borst P. Tissue distribution of the human MDR3 P-glycoprotein. Lab. Invest. 1994; 71:638–649. [PubMed: 7734012]

(4). Cordon-Cardo C, O’Brien JP, Boccia J, Casals D, Bertino JR, Melamed MR. Expression of the multidrug resistance gene product (P-glycoprotein) in human normal and tumor tissues. J. Histochem. Cytochem. 1990; 38:1277–1287. [PubMed: 1974900]

(5). Gottesman MM, Fojo T, Bates SE. Multidrug resistance in cancer: Role of ATP-dependent transporters. Nat. Rev. Cancer. 2002; 2:48–58. [PubMed: 11902585]

(6). McDevitt CA, Callaghan R. How can we best use structural information on P-glycoprotein to design inhibitors? Pharmacol. Ther. 2007; 113:429–441. [PubMed: 17208306]

(7). Choudhuri S, Klaassen CD. Structure, function, expression, genomic organization, and single nucleotide polymorphisms of human ABCB1 (MDR1), ABCC (MRP), and ABCG2 (BCRP) efflux transporters. Int. J. Toxicol. 2006; 25:231–259. [PubMed: 16815813]

(8). Ayesh S, Shao YM, Stein WD. Co-operative, competitive and non-competitive interactions between modulators of P-glycoprotein. Biochim. Biophys. Acta. 1996; 1316:8–18. [PubMed: 8634345]

(9). Ferry DR, Russell MA, Cullen MH. P-Glycoprotein possesses a 1,4-dihydropyridine-selective drug acceptor site which is allosterically coupled to a vinca-alkaloid-selective binding site. Biochem. Biophys. Res. Commun. 1992; 188:440–445. [PubMed: 1358068]

(10). Pascaud C, Garrigos M, Orlowski S. Multidrug resistance transporter P-glycoprotein has distinct but interacting binding sites for cytotoxic drugs and reversing agents. Biochem. J. 1998; 333(part 2):351–358. [PubMed: 9657975]

(11). Shapiro AB, Ling V. Positively cooperative sites for drug transport by P-glycoprotein with distinct drug specificities. Eur. J. Biochem. 1997; 250:130–137. [PubMed: 9432000]

(12). Loo TW, Bartlett MC, Clarke DM. Transmembrane segment 1 of human P-glycoprotein contributes to the drug-binding pocket. Biochem. J. 2006; 396:537–545. [PubMed: 16492138]

(13). Loo TW, Bartlett MC, Clarke DM. Transmembrane segment 7 of human P-glycoprotein forms part of the drug-binding pocket. Biochem. J. 2006; 399:351–359. [PubMed: 16813563]

(14). Pleban K, Kopp S, Csaszar E, Peer M, Hrebicek T, Rizzi A, Ecker GF, Chiba P. P-Glycoprotein substrate binding domains are located at the transmembrane domain/transmembrane domain interfaces: A combined photoaffinity labeling-protein homology modeling approach. Mol. Pharmacol. 2005; 67:365–374. [PubMed: 15509712]

(15). Rothnie A, Storm J, Campbell J, Linton KJ, Kerr ID, Callaghan R. The topography of transmembrane segment six is altered during the catalytic cycle of P-glycoprotein. J. Biol. Chem. 2004; 279:34913–34921. [PubMed: 15192095]

(16). Rosenberg MF, Kamis AB, Callaghan R, Higgins CF, Ford RC. Three-dimensional structures of the mammalian multidrug resistance P-glycoprotein demonstrate major conformational changes in the transmembrane domains upon nucleotide binding. J. Biol. Chem. 2003; 278:8294–8299. [PubMed: 12501241]

(17). Mechetner EB, Schott B, Morse BS, Stein WD, Druley T, Davis KA, Tsuruo T, Roninson IB. P-Glycoprotein function involves conformational transitions detectable by differential immunoreactivity. Proc. Natl. Acad. Sci. U.S.A. 1997; 94:12908–12913. [PubMed: 9371774]

(18). Nagy H, Goda K, Arceci R, Cianfriglia M, Mechetner E, Szabo G Jr. P-Glycoprotein conformational changes detected by antibody competition. Eur. J. Biochem. 2001; 268:2416–2420. [PubMed: 11298761]

(19). Julien M, Gros P. Nucleotide-induced conformational changes in P-glycoprotein and in nucleotide binding site mutants monitored by trypsin sensitivity. Biochemistry. 2000; 39:4559–4568. [PubMed: 10758006]

(20). Loo TW, Clarke DM. Inhibition of oxidative cross-linking between engineered cysteine residues at positions 332 in predicted transmembrane segments (TM) 6 and 975 in predicted TM12 of human P-glycoprotein by drug substrates. J. Biol. Chem. 1996; 271:27482–27487. [PubMed: 8910331]

(21). Loo TW, Clarke DM. Drug-stimulated ATPase activity of human P-glycoprotein requires movement between transmembrane segments 6 and 12. J. Biol. Chem. 1997; 272:20986–20989. [PubMed: 9261097]

(22). Martin C, Berridge G, Mistry P, Higgins C, Charlton P, Callaghan R. The molecular interaction of the high affinity reversal agent XR9576 with P-glycoprotein. Br. J. Pharmacol. 1999; 128:403–411. [PubMed: 10510451]

(23). Martin C, Higgins CF, Callaghan R. The vinblastine binding site adopts high- and low-affinity conformations during a transport cycle of P-glycoprotein. Biochemistry. 2001; 40:15733–15742. [PubMed: 11747450]

(24). Rosenberg MF, Velarde G, Ford RC, Martin C, Berridge G, Kerr ID, Callaghan R, Schmidlin A, Wooding C, Linton KJ, Higgins CF. Repacking of the transmembrane domains of P-glycoprotein during the transport ATPase cycle. EMBO J. 2001; 20:5615–5625. [PubMed: 11598005]

(25). Callaghan R, Ford RC, Kerr ID. The translocation mechanism of P-glycoprotein. FEBS Lett. 2006; 580:1056–1063. [PubMed: 16380120]

(26). Liu CE, Ames GF. Characterization of transport through the periplasmic histidine permease using proteoliposomes reconstituted by dialysis. J. Biol. Chem. 1997; 272:859–866. [PubMed: 8995374]

(27). Tombline G, Bartholomew LA, Urbatsch IL, Senior AE. Combined mutation of catalytic glutamate residues in the two nucleotide binding domains of P-glycoprotein generates a conformation that binds ATP and ADP tightly. J. Biol. Chem. 2004; 279:31212–31220. [PubMed: 15159388]

(28). Dawson RJ, Locher KP. Structure of a bacterial multidrug ABC transporter. Nature. 2006; 443:180–185. [PubMed: 16943773]

(29). Loo TW, Clarke DM. Functional consequences of phenylalanine mutations in the predicted transmembrane domain of P-glycoprotein. J. Biol. Chem. 1993; 268:19965–19972. [PubMed: 8104183]

(30). Devine SE, Ling V, Melera PW. Amino acid substitutions in the sixth transmembrane domain of P-glycoprotein alter multidrug resistance. Proc. Natl. Acad. Sci. U.S.A. 1992; 89:4564–4568. [PubMed: 1350094]

(31). Song J, Melera PW. Further characterization of the sixth transmembrane domain of Pgp1 by site-directed mutagenesis. Cancer Chemother. Pharmacol. 2001; 48:339–346. [PubMed: 11761450]

(32). Ecker GF, Csaszar E, Kopp S, Plagens B, Holzer W, Ernst W, Chiba P. Identification of ligand-binding regions of P-glycoprotein by activated-pharmacophore photoaffinity labeling and matrix-assisted laser desorption/ionization-time-of-flight mass spectrometry. Mol. Pharmacol. 2002; 61:637–648. [PubMed: 11854445]

(33). Greenberger LM. Major photoaffinity drug labeling sites for iodoaryl azidoprazosin in P-glycoprotein are within, or immediately C-terminal to, transmembrane domains 6 and 12. J. Biol. Chem. 1993; 268:11417–11425. [PubMed: 8098711]

(34). Loo TW, Clarke DM. Mutations to amino acids located in predicted transmembrane segment 6 (TM6) modulate the activity and substrate specificity of human P-glycoprotein. Biochemistry. 1994; 33:14049–14057. [PubMed: 7947814]

(35). Loo TW, Clarke DM. Defining the drug-binding site in the human multidrug resistance P-glycoprotein using a methanethiosulfonate analog of verapamil, MTS-verapamil. J. Biol. Chem. 2001; 276:14972–14979. [PubMed: 11279063]

(36). Zhang X, Collins KI, Greenberger LM. Functional evidence that transmembrane 12 and the loop between transmembrane 11 and 12 form part of the drug-binding domain in P-glycoprotein encoded by MDR1. J. Biol. Chem. 1995; 270:5441–5448. [PubMed: 7890659]

(37). Storm J, Modok S, O'Mara ML, Tieleman DP, Kerr ID, Callaghan R. Cytosolic region of TM6 in P-glycoprotein:Topographical analysis and functional perturbation by site directed labeling. Biochemistry. 2008; 47:3615–3624. [PubMed: 18303860]

(38). Storm J, O'Mara ML, Crowley EH, Peall J, Tieleman DP, Kerr ID, Callaghan R. Residue G346 in transmembrane segment six is involved in inter-domain communication in P-glycoprotein. Biochemistry. 2007; 46:9899–9910. [PubMed: 17696319]

(39). Taylor AM, Storm J, Soceneantu L, Linton KJ, Gabriel M, Martin C, Woodhouse J, Blott E, Higgins CF, Callaghan R. Detailed characterization of cysteine-less P-glycoprotein reveals subtle pharmacological differences in function from wild-type protein. Br. J. Pharmacol. 2001; 134:1609–1618. [PubMed: 11739236]

(40). Hoedemaeker FJ, Signorelli T, Johns K, Kuntz DA, Rose DR. A single chain Fv fragment of P-glycoprotein-specific monoclonal antibody C219. Design, expression, and crystal structure at 2.4 Å resolution. J. Biol. Chem. 1997; 272:29784–29789. [PubMed: 9368049]

(41). Bradford MM. A rapid and sensitive method for the quantitation of microgram quantities of protein utilizing the principle of protein–dye binding. Anal. Biochem. 1976; 72:248–254. [PubMed: 942051]

(42). Chifflet S, Torriglia A, Chiesa R, Tolosa S. A method for the determination of inorganic phosphate in the presence of labile organic phosphate and high concentrations of protein: Application to lens ATPases. Anal. Biochem. 1988; 168:1–4. [PubMed: 2834977]

(43). Martin C, Berridge G, Higgins CF, Callaghan R. The multi-drug resistance reversal agent SR33557 and modulation of vinca alkaloid binding to P-glycoprotein by an allosteric interaction. Br. J. Pharmacol. 1997; 122:765–771. [PubMed: 9375975]

(44). O'Mara ML, Tieleman DP. P-glycoprotein models of the apo and ATP-bound states based on homology with Sav1866 and MalK. FEBS Lett. 2007; 581:4217–4222. [PubMed: 17706648]

(45). Guex N, Peitsch MC. SWISS-MODEL and the Swiss-PdbViewer: An environment for comparative protein modeling. Electrophoresis. 1997; 18:2714–2723. [PubMed: 9504803]

(46). Aller SG, Yu J, Ward A, Weng Y, Chittaboina S, Zhuo R, Harrell PM, Trinh YT, Zhang Q, Urbatsch IL, Chang G. Structure of P-glycoprotein reveals a molecular basis for poly-specific drug binding. Science. 2009; 323:1718–1722. [PubMed: 19325113]

(47). Loo TW, Clarke DM. Identification of residues in the drug-binding site of human P-glycoprotein using a thiol-reactive substrate. J. Biol. Chem. 1997; 272:31945–31948. [PubMed: 9405384]

(48). Berridge G, Walker JA, Callaghan R, Kerr ID. The nucleotide-binding domains of P-glycoprotein. Functional symmetry in the isolated domain demonstrated by *N*-ethylmaleimide labelling. Eur. J. Biochem. 2003; 270:1483–1492. [PubMed: 12654004]

(49). Davidson AL, Nikaido H. Purification and characterization of the membrane-associated components of the maltose transport system from Escherichia coli. J. Biol. Chem. 1991; 266:8946–8951. [PubMed: 2026607]

(50). Ko YH, Pedersen PL. The first nucleotide binding fold of the cystic fibrosis transmembrane conductance regulator can function as an active ATPase. J. Biol. Chem. 1995; 270:22093–22096. [PubMed: 7545672]

(51). Nikaido K, Liu PQ, Ames GF. Purification and characterization of HisP, the ATP-binding subunit of a traffic ATPase (ABC transporter), the histidine permease of Salmonella typhimurium. Solubility, dimerization, and ATPase activity. J. Biol. Chem. 1997; 272:27745–27752. [PubMed: 9346917]

(52). Sonveaux N, Vigano C, Shapiro AB, Ling V, Ruysschaert JM. Ligand-mediated tertiary structure changes of reconstituted P-glycoprotein. A tryptophan fluorescence quenching analysis. J. Biol. Chem. 1999; 274:17649–17654. [PubMed: 10364203]

(53). Martin C, Berridge G, Higgins CF, Mistry P, Charlton P, Callaghan R. Communication between multiple drug binding sites on P-glycoprotein. Mol. Pharmacol. 2000; 58:624–632. [PubMed: 10953057]

Europe PMC Funders Author Manuscripts

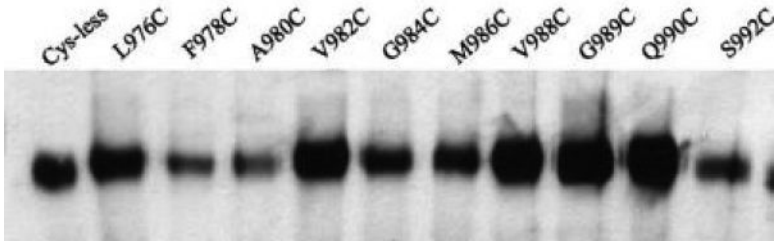

Figure 1.
Expression of ABCB1 in high-five insect cells. A representative immunoblot of the expression of ABCB1 mutant isoforms expressed in high-five cells. ABCB1 expression was detected following SDS–PAGE on 7.5% (w/v) acrylamide gels and immunoblotting with the monoclonal antibody C219. The total amount of protein loaded onto each lane was 15 μg.

Europe PMC Funders Author Manuscripts

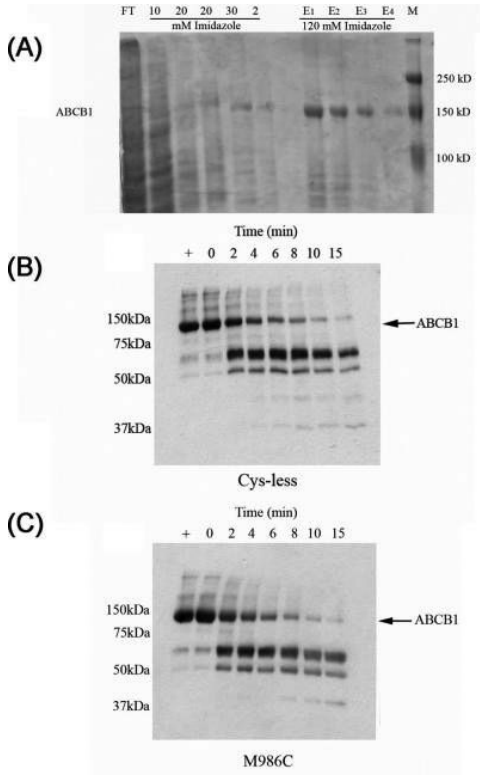

Figure 2.

Purification and partial proteolysis of ABCB1 isoforms. (A) ABCB1 mutant isoforms were extracted from insect cell membranes by 2% (w/v) octyl-glucoside, purified by immobilized metal-affinity chromatography, and analyzed by SDS–PAGE. FT denotes the flow through, and the following five lanes represent the wash steps (up to 30 mM imidazole) to remove protein bound weakly to the resin. E1–E4 represent four elution steps at 120 mM imidazole. ABCB1 is indicated by an arrow, and M denotes the molecular marker. Proteolysis of purified, reconstituted Cys-less (B) and M986C (C) was carried out in the presence of 0.5 μg of bovine pancreatic trypsin. Time denotes the incubation period of the protein with trypsin at 37 °C (see the Materials and Methods). Protein was detected using C219 antibody following immunoblotting. Undigested ABCB1 is indicated by the arrow. The positive control corresponds to no proteolytic digestion by trypsin.

Europe PMC Funders Author Manuscripts

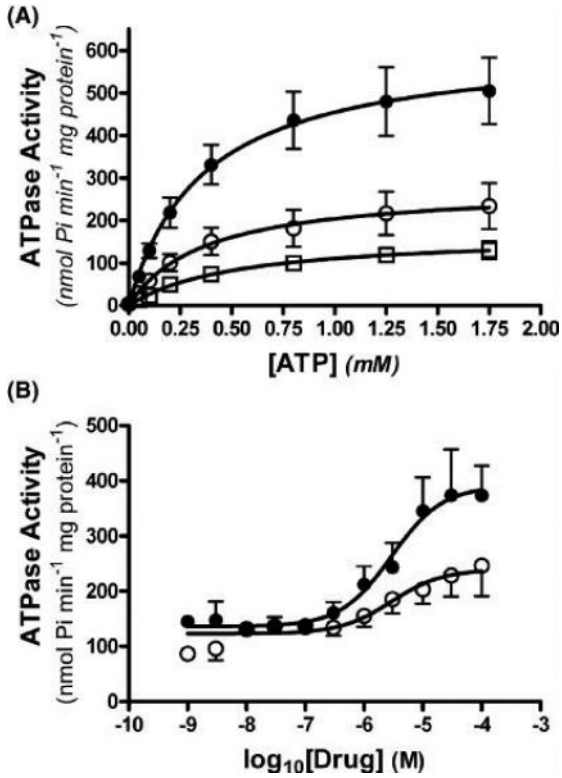

Figure 3.

ATPase activity of cysteine-less ABCB1 isoform. ATP hydrolysis of purified, reconstituted cysteine-less ABCB1 was measured using a colorimetric assay that detects the release of inorganic phosphate. (A) Activity was measured as a function of the ATP concentration (0–1.75 mM) for cysteine-less ABCB1 in the absence (□) or presence of nicardipine (●) or vinblastine (○). (B) Activity was measured as a function of either the nicardipine (●) or vinblastine (○) concentration at 2 mM ATP. Nonlinear least-squares regression was used to fit the Michaelis–Menten equation (A) or the general dose–response equation (B) to the data. Values represent the mean ± standard error of the mean (SEM) obtained from at least four independent protein preparations.

Europe PMC Funders Author Manuscripts

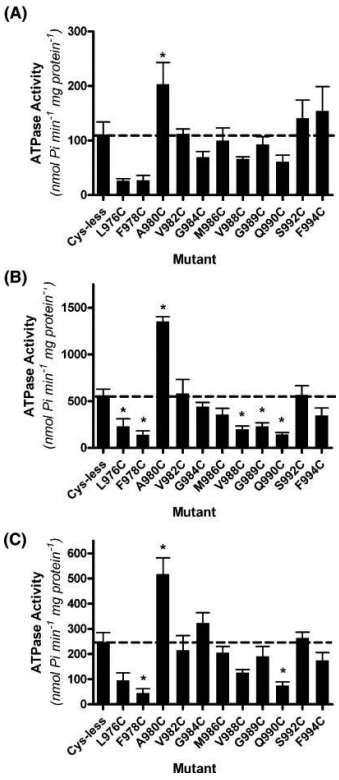

Figure 4.

Maximal ATPase activity of TM12 mutant isoforms. ATPase activity of the mutant isoforms was determined under basal (A) and drug-stimulated conditions (B, nicardipine; C, vinblastine). The maximal ATPase activity (V_{max}) was determined from Michaelis–Menten curves (comparable to those in Figure 3) and is represented for each isoform in the form of a bar chart. The values represent the mean ± SEM of at least three independent purifications, and an asterisk refers to a statistically significant difference ($p<0.05$) compared to the Cys-less isoform.

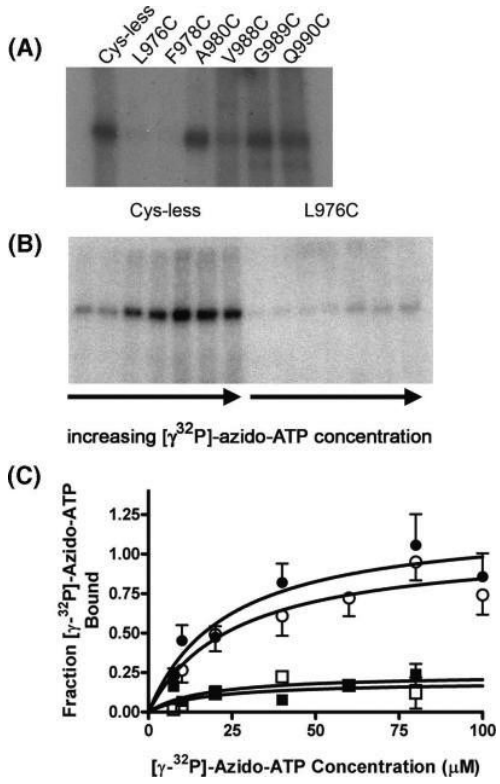

Figure 5.

Nucleotide binding to TM12 mutant isoforms. Mutant isoforms (0.3 μg) were incubated with [γ-^{32}P]-azido-ATP; cross-linked protein was resolved using SDS–PAGE; and the amount of bound radiolabel was detected by autoradiography. (A) Representative autoradiogram showing altered binding of [γ-^{32}P]-azido-ATP (10 μM) to isoforms. (B) Autoradiograms showing the binding of [γ-^{32}P]-azido-ATP (10–100 μM) to the purified, reconstituted cysteine-less and L976C mutant isoforms. (C) Data obtained for the cysteine-less, L976C, F978C, and A980C isoforms were analyzed by densitometry, and the amount bound was plotted as a function of the [γ-^{32}P]-azido-ATP concentration. Nonlinear least-squares regression was used to fit the Langmuir binding isotherm to the data. The values represent the mean ± SEM obtained from at least three independent protein preparations.

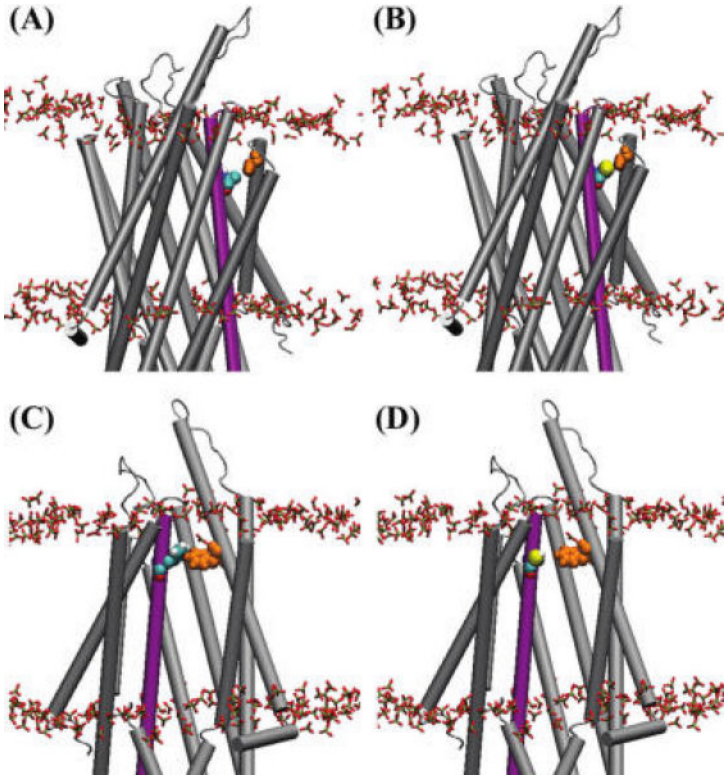

Figure 6.

In silico TM12 mutations. In each case, TM12 is colored purple and the head groups of the POPE bilayer are shown in CPK liquorice representations. The remaining TM helices are shaded gray, unless otherwise specified. Water in the substrate translocation pore and associated with TM protein is rendered blue. (A) Wild-type A980 (CPK spacefill) is located in the TM9–TM12 cleft and has no significant protein interactions. (B) Mutation to A980C allows for hydrogen bonding to S850 (orange), increasing TM12–TM9 contacts. (C) F978 (CPK spacefill) is located on the TM12–TM1 helix–helix interface and hydrogen bonds with F72 (orange). (D) Mutation to F978C (CPK) prevents hydrogen bonding to F72.

Europe PMC Funders Author Manuscripts

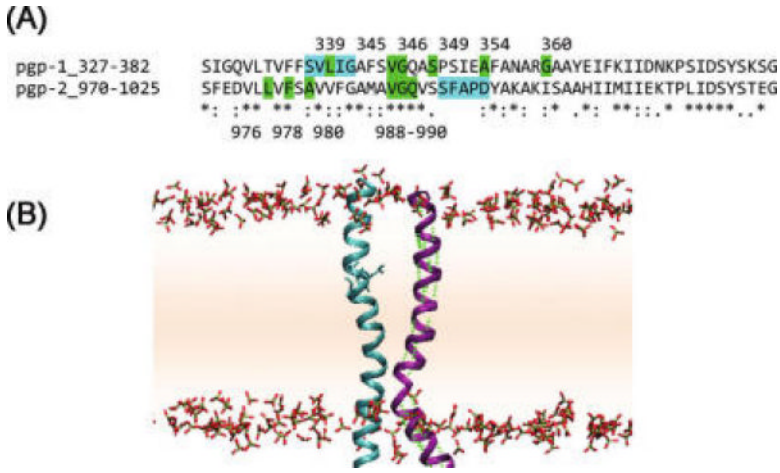

Figure 7.

Sequence alignment and hydrogen-bonding profile of TM6 and TM12 through the membrane. (A) Sequence alignment of ABCB1 TM6/ICL3 and TM12/ICL6 shows a very high level of sequence conservation between the two regions, with approximately 80% sequence similarity and 45% sequence identity. Mutations altering ATPase activity are shaded green and numbered. The proposed TM6 and TM12 hinges are shaded cyan. Identical residues are marked with an asterisk, conserved residues are identified by ":" or "." depending upon the degree of sequence conservation. (B) Side profile of TM12 (purple) shows only one major disruption in the normal α-helical hydrogen-bonding pattern (green dashed lines), corresponding to a marked kink in TM12 located near the cytoplasmic lipid–water interface. TM6 is shown for reference, and the residues implicated in the TM6 hinge (cyan) and the POPE head groups (CKP coloring) are illustrated in liquorice representation.

Europe PMC Funders Author Manuscripts

Europe PMC Funders Author Manuscripts

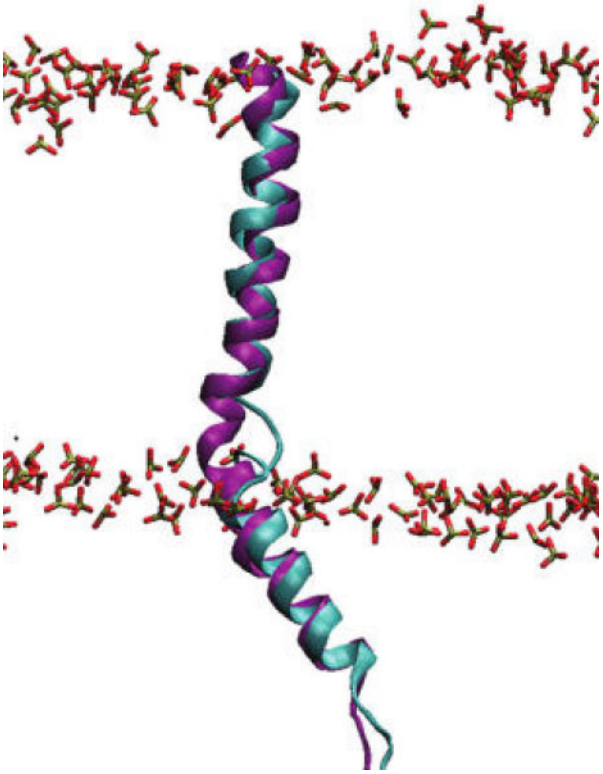

Figure 8.
Comparison of the lipid-embedded human TM12 homology model and TM12 from the mouse P-glycoprotein A crystal structure. A comparison of the lipid-embedded human TM12 homology model (purple) and TM12 from the mouse P-glycoprotein A crystal structure (cyan). Both the TM12 homology model and crystal structure show a marked kink near the intracellular lipid–water interface, corresponding to the conserved sequence motif SSFAPD found in both humans (S992–D997) and mice (V988–S993). Here, the lipid phosphates are shown as stick representations.

Europe PMC Funders Author Manuscripts

Table 1

Mutagenic Oligonucleotide Primers Used To Generate TM12 Mutations[a]

mutation	primer sequence (5′–3′)	diagnostic restriction digest
L976C	GAGGATGTTCTA**tgt**GTATTTTCAGCTGTTG	−*Spe*I
F978C	GTTCTACTAGTA**TgT**TCtGCaGTTGTCTTTGGTG	+*Pst*I
A980C	CTACTAGTATTTTCA**tgc**GTTGTCTTTGGTGCCATGGCC	−*Pvu*II
V982C	CTAGTATTTTCAGCgGTT**tgC**TTTGGTGCCATGGCC	−*Pvu*II
G984C	GCTGTTGTCTTT**tGT**GCtATGGCCGTGG	−*Nco*I
M986C	GTATTTGGTGC**ttgt**GCtGTGGGGCAAGTC	−*Nco*I
V988C	GGTGCCATGGCC**tgt**GGGCAAGTCAGTTC	−*Bst*XI
G989C	CTTTGGTGCCATGGCCGTG**tGc**CAAGTCAGTTCATTTGC	+*Bst*XI
Q990C	GGCCGTGGGG**tgt**GTCtcTTCATTTGCTCC	+*Ear*I

[a]Primer sequences contain an introduced cysteine residue (bold) and additional silent mutations (lower case), with respect to the coding sequence that generates or removes the indicated restriction site.

Table 2

Potency and Degree of Drug Stimulation of ATP Hydrolysis by ABCB1[a]

	nicardipine		vinblastine	
	EC_{50} (μM)	**fold stimulation**	**EC_{50} (μM)**	**fold stimulation**
Cys-less	4.1±1.1	4.0±0.6	5.91±2.9	2.2±0.2
L976C	5.2±0.2	7.4±1.4	10.0±0.0	3.5±0.6
F978C	24.1±2.3[b]	9.5±1.4	42.9±4.3[b]	2.3±0.5
A980C	3.4±0.3	5.1±0.9	12.3±1.8	3.2±0.8
V982C	5.8±0.9	4.2±0.5	2.0±0.7	1.8±0.2
G984C	37.6±11.2[b]	16.2±6.6[b]	6.7±1.7	6.2±2.3
M986C	9.2±0.8	4.7±1.1	15.0±2.0[b]	2.8±0.7
V988C	3.9±0.6	3.1±0.1	7.3±2.3	1.9±0.2
G989C	13.6±1.5	5.1±1.6	4.9±0.9	2.4±0.3
Q990C	6.9±1.1	3.7±1.0	ND[c]	ND[c]
S992C	4.9±0.5	4.2±0.6	7.1±2.6	2.3±0.4
F994C	1.7±0.4	3.2±0.8	5.9±2.5	1.6±0.3

[a] ATPase activity was plotted as a function of the drug concentration and potency (EC_{50}) and degree of stimulation obtained by nonlinear regression of the dose–response relationship equation. Values represent the mean±SEM of at least three independent purifications.

[b] A significant difference ($p<0.05$) compared to the Cys-less isoform.

[c] ND corresponds to not detected.

Table 3

Nucleotide Binding to ABCB1[a]

ABCB1 isoform	[^{32}P]-N3-ATP	[^{32}P]-N3-ATP+ 1 mM ATP	[^{32}P]-N3-ATP+ 1 mM ADP
Cys-less	1.00	0.21±0.05	0.23±0.06
L976C	0.21±0.05	0.10±0.02	0.05±0.03
F978C	0.07±0.01	ND	ND
A980C	1.81±0.71	0.45±0.10	0.15±0.08
V988C	0.53±0.20	ND	ND
G989C	0.83±0.04	0.10±0.05	0.13±0.06
Q990C	1.05±0.30	0.19±0.11	0.01±0.01

[a]The ABCB1 isoforms were incubated with 10 μM [γ^{32}P]-azido-ATP in the presence or absence of excess unlabeled nucleotides (1 mM). The incubations were performed under conditions that did not support ATP hydrolysis, and proteins were photolabeled as described in the Materials and Methods. The relative binding intensities were estimated by densitometric analysis of autoradiograms, and the value obtained for cysteine-less ABCB1 in the absence of excess nucleotide was assigned a value of 1. Values correspond to mean ± SEM obtained from a minimum of four independent protein preparations.